REFERENCES

[1] A. S. Templin and R. L. Gunshor, "Analytical model for varactor-tuned waveguide Gunn oscillator," *IEEE Trans. Microwave Theory Tech.*, vol. MTT-22, pp. 554–556, May 1974.
[2] M. Dean and M. Howes, "Electronic tuning of stable transferred electron oscillators," *IEEE Trans. Electron Devices*, vol. ED-21, pp. 563–570, Sept. 1974.
[3] R. L. Eisenhart and P. J. Khan, "Theoretical and experimental analysis of a waveguide mounting structure," *IEEE Trans. Microwave Theory Tech.*, vol. MTT-19, pp. 706–719, Aug. 1971.
[4] N. Marcuvitz, *Waveguide Handbook* (M.I.T. Rad. Lab. Ser. vol. 10). New York: McGraw-Hill, 1951.
[5] O. L. El-Sayed, "Impedance characterization of a two-post mounting structure for varactor tuned Gunn-oscillators," *IEEE Trans. Microwave Theory Tech.*, vol. MTT-22, pp. 769–776, Aug. 1974.
[6] K. Chang and P. J. Khan, "Coupling between narrow transverse inductive strips in waveguide," *IEEE Trans. Microwave Theory Tech.*, vol. MTT-24, pp. 101–105, Feb. 1976.
[7] J. S. Joshi and J. A. F. Cornick, "Analysis of a waveguide mounting configuration for electronically tuned transferred-electron-device oscillators and its circuit application," *IEEE Trans. Microwave Theory Tech.*, vol. MTT-24, pp. 573–584, Sept. 1976.
[8] R. L. Eisenhart, "Comments on a 2-gap waveguide mount," International Microwave Symposium, June 1976.
[9] V. H. Rumsey, "The reaction concept in electromagnetic theory," *Phys. Rev.*, ser. 2, vol. 94, pp. 1483–1491, June 15, 1954.
[10] R. F. Harrington, *Time Harmonic Electromagnetic Fields*. New York: McGraw-Hill, 1961.

Analysis of Waveguide Post Configurations: Part II—Dual-Gap Cases

J. S. JOSHI AND J. A. F. CORNICK

***Abstract*—The analysis given in Part I [1] is applied to two particular structures of general interest. The first is the two-post case, each post having one gap, and the second is the single-post with two gaps. The impedance or admittance matrix elements are used to construct the gap port networks which are then used to obtain the waveguide obstacle representations. These latter representations are used to obtain experimental confirmation of the analysis.**

INTRODUCTION

THE general two-post and single-post two-gap structures in infinite rectangular waveguide are of special significance in the design of microwave solid-state sources. The gap immittance matrices derived in [1] are applied here to these specific cases. First, the nature of the coupling network between the two-gap ports is discussed, and these coupling networks are then used to derive the impedance presented by the post structure to the dominant H_{10} mode in the guide. Results of experimental work carried out on some general post arrangements are also included in support of the theory. The relevant matrix expressions derived in [1] are given here for convenient reference with all the quantities defined.

For the structure of Fig. 1(a),

$$Z_{ijn} = \sum_{m=1}^{\infty} Z_{mn} \left(\frac{k_{ipm} k_{jpm}}{k_{ign} k_{jgn}} \right) \exp\left(-\Gamma_{mn} L_{ij}\right) \qquad (1)$$

and for the structure of Fig. 1(b),

$$Y_{ijn} = \left[\sum_{m=1}^{\infty} Z_{mn} \left(\frac{k_{pm}^2}{k_{ign} k_{jgn}} \right) \right]^{-1} \qquad (2)$$

where

$$Z_{mn} = j\eta \frac{b}{a} \frac{(k^2 - k_y^2)}{(2 - \delta_n)k} \frac{1}{\Gamma_{mn}}$$

$$k_{ipm} = \sin k_x s_i \frac{\sin \theta_{im}}{\theta_{im}} \qquad k_{ign} = \cos k_y h_i \frac{\sin \phi_{in}}{\phi_{in}}$$

$$\theta_{im} = \frac{m\pi w_i}{2a} \qquad \phi_{in} = \frac{n\pi g_i}{2b} \qquad w_i = 1.8 d_i$$

$$k_x = \frac{m\pi}{a} \qquad k_y = \frac{n\pi}{b} \qquad k = \frac{2\pi}{\lambda}$$

$$\Gamma_{mn} = (k_x^2 + k_y^2 - k^2)^{1/2}$$

$$\delta_n = 1, \quad \text{for } n = 0$$

$$= 0, \quad \text{for } n \neq 0, \qquad i,j = 1,2.$$

THE TWO-POST STRUCTURE

The elements of the impedance matrix for an nth spatial harmonic mode given by (1) can be used to construct the coupling network between the two-gap ports. This network is preferred in T form since impedance elements are considered. All the various mode pair impedance ports for $m = 1$–∞ for the given value of n are coupled to the two-gap ports through the post and gap coupling factors and the exponential distance factors.

Manuscript received March 30, 1976; revised August 2, 1976. This work forms part of the Ph.D. dissertation submitted by J. S. Joshi to the Council for National Academic Awards, London, England (May 1976).

The authors are with Mullard (Hazel Grove) Ltd., Bramhall Moor Lane, Hazel Grove, Stockport, Cheshire, England.

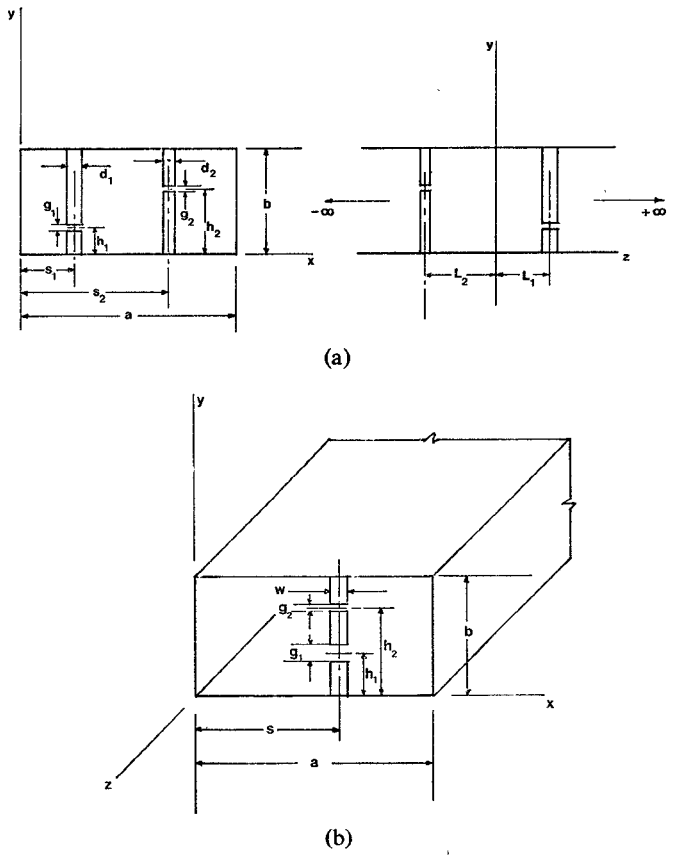

Fig. 1. Waveguide post configurations. (a) Two-post configuration. (b) Single-post two-gap configuration.

By symmetrical location of post geometry parameters, it is possible to decouple a set of Z_{mn} mode pair impedance ports (for various m values) from the elements of the T or π network between the two-gap ports [2].

Post Structure Obstacle Representation

The coupling network representation can be used to derive the obstacle impedance of the post structure for a general (m,n) mode, but the dominant H_{10} mode is, however, of the most significance, and a knowledge of this impedance is necessary for the experimental verification.

The procedure for obtaining the obstacle representation is as follows. Firstly, the two characteristic impedance ports (in this case the Z_{c10} ports) corresponding to the two waveguide arms are isolated. The remaining spatial harmonic impedance components and the gap terminations are combined in a suitable form. The total network appearing between the two identifiable waveguide arms represents the obstacle impedance. Unlike the previous special cases of single post or coplanar posts which could be represented by a shunt obstacle impedance at the $z = 0$ post plane, the general case of the staggered posts means that the obstacle network must take into account the separation of the posts in the z direction. The representation would therefore be a general two-port network, the two waveguide ports being coincident with the individual post planes. The general staggered post case is considered first, and the coplanar case is dealt with subsequently.

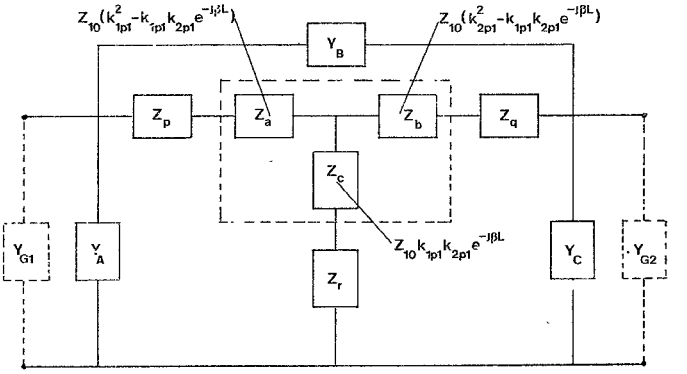

Fig. 2. Coupling network between the gap ports for the general two-post configuration.

The Staggered Post Case: Referring to Fig. 2, a T network is introduced between the two-gap ports for $n = 0$, separating each arm of the T into elements $Z(abc)$ for which $m = 1$ and elements $Z(pqr)$ which are the result of the summation over $m = 2$–∞. Using (1) and the simple relation between the Z-matrix elements and the elements of the T network then,

$$Z_a = Z_{10}\{k_{1p1}^2 - k_{1p1}k_{2p1} \exp(-j\beta L)\}$$

$$Z_b = Z_{10}\{k_{2p1}^2 - k_{1p1}k_{2p1} \exp(-j\beta L)\}$$

$$Z_c = Z_{10}k_{1p1}k_{2p1} \exp(-j\beta L)$$

$$Z_p = \sum_{m=2}^{\infty} Z_{m0}\{k_{1pm}^2 - k_{1pm}k_{2pm} \exp(-\Gamma_{m0}L)\}$$

$$Z_q = \sum_{m=2}^{\infty} Z_{m0}\{k_{2pm}^2 - k_{1pm}k_{2pm} \exp(-\Gamma_{m0}L)\}$$

$$Z_r = \sum_{m=2}^{\infty} Z_{m0}k_{1pm}k_{2pm} \exp(-\Gamma_{m0}L)$$

where

$$Z_{10} = \eta \frac{b}{a}\frac{k}{\beta} = \frac{1}{2}Z_{c10}$$

$$\beta = -j\Gamma_{10} = \sqrt{\left\{\left(\frac{2\pi}{\lambda}\right)^2 - \left(\frac{\pi}{a}\right)^2\right\}}.$$

For $n > 0$, using (1) for the basic Z-matrix elements, the simple T to π transformation and the adding of all such π-network elements in parallel results in $Y(ABC)$ values in Fig. 2 given by

$$Y_A = \sum_{n=1}^{\infty}\left[\frac{Z_{22n} - Z_{12n}}{(Z_{11n}Z_{22n} - Z_{12n}^2)}\right]$$

$$Y_B = \sum_{n=1}^{\infty}\left[\frac{Z_{12n}}{(Z_{11n}Z_{22n} - Z_{12n}^2)}\right]$$

$$Y_C = \sum_{n=1}^{\infty}\left[\frac{Z_{11n} - Z_{12n}}{(Z_{11n}Z_{22n} - Z_{12n}^2)}\right]$$

The network of Fig. 2 is completed by the addition of the gap port terminating admittances Y_{G1}, Y_{G2}.

The T network $Z(abc)$ of Fig. 2 takes into account the various couplings to (1,0) waveguide ports. In order to

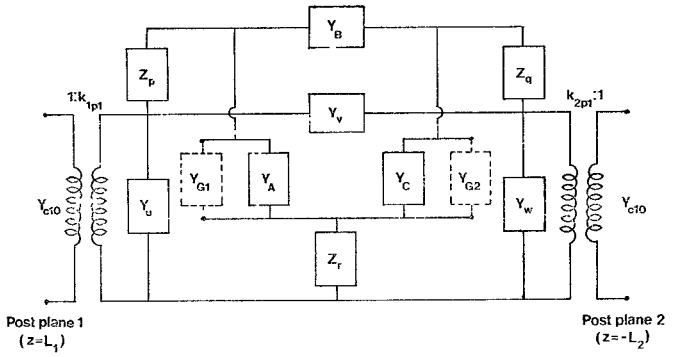

Fig. 3. Obstacle network representation of the post configuration of Fig. 1(a) to the incident H_{10} mode in the waveguide.

isolate the (1,0) port and split it into the characteristic ports, this T network is converted to its π equivalent. When the admittance elements in this π network are separated into real and imaginary components then,

$$Y_a' = \frac{1}{2Z_{10}k_{1p1}^2} + Y_u = \frac{Y_{c10}}{k_{1p1}^2} + Y_u$$

$$Y_b' = 0 + Y_v$$

$$Y_c' = \frac{1}{2Z_{10}k_{1p1}^2} + Y_w = \frac{Y_{c10}}{k_{1p1}^2} + Y_w$$

where

$$Y_u = jY_{c10}\left\{\frac{1}{k_{1p1}k_{2p1}\sin\beta L} - \frac{1}{k_{1p1}^2\tan\beta L}\right\}$$

$$Y_v = -jY_{c10}\frac{1}{k_{1p1}k_{2p1}\sin\beta L}$$

$$Y_w = jY_{c10}\left\{\frac{1}{k_{1p1}k_{2p1}\sin\beta L} - \frac{1}{k_{2p1}^2\tan\beta L}\right\}.$$

The conductance terms of Y_a' and Y_c' correspond to the transformation of the waveguide characteristic admittances Y_{c10} for the H_{10} mode through transformers of turns ratios k_{1p1} and k_{2p1} for posts 1 and 2, respectively. The complete obstacle network can thus be drawn as in Fig. 3 with the two waveguide port locations coincident with posts 1 and 2, respectively. The form of the network given in Fig. 3 is useful to examine the significance of the various elements and the consideration of special cases.

Components of the General Obstacle Network: The post structure obstacle network of Fig. 3 takes into account the effect of all possible modes involved in the interaction of the two posts. Here are considered the effects of individual parameters and some special cases.

The effect of evanescent mode coupling for $n > 0$ spatial harmonics between the two-post structures is taken into account by the admittance elements $Y(ABC)$. These elements contain the post separation term $\exp(-\Gamma_{mn}L)$, and thus the effect of the staggered post location is taken into account.

The elements $Z(pqr)$ account for the evanescent modes corresponding to $n = 0, m > 1$, the staggered post location effect being via the $\exp(-\Gamma_{m0}L)$ term. When the two-gap

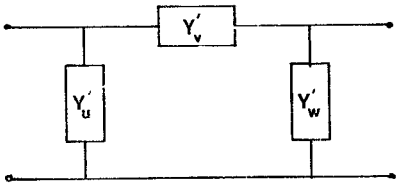

Fig. 4. H_{10} mode coupling network for the symmetrical staggered two-post arrangement.

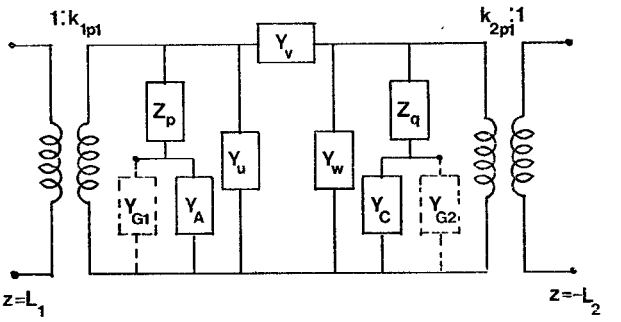

Fig. 5. Obstacle network for large post separation.

ports are short circuited, resulting in two complete posts, the evanescent mode coupling between the two posts for $n > 0$ is eliminated. The elements $Z(pqr)$ plus $Y(uvw)$ then form the obstacle network.

The dominant H_{10} mode coupling between the two posts is accounted for by the admittance elements $Y(uvw)$. The coupling is modified by the post axes locations and diameters, i.e., by the post coupling factors k_{1p1} and k_{2p1}. The symmetrical case $s_1 = a - s_2 = s$ and $k_{1p1} = k_{2p1} = k_{p1}$ results in the dominant mode coupling network of Fig. 4 with the element values $Y'(uvw)$ given by

$$Y_u' = Y_w' = \frac{jY_{c10}\tan\beta L/2}{k_{p1}^2} \qquad Y_v' = -j\frac{Y_{c10}\csc\beta L}{k_{p1}^2}.$$

Except for the k_{p1}^2 factor, which accounts for the post axis position, this coupling network is the same as the equivalent network of a uniform transmission line of length L and characteristic admittance Y_{c10}. This effect is independent of the gap locations.

When the separation between the two posts is large such that $\exp(-\Gamma_{mn}L) \to 0$, all the higher order mode coupling between the two posts vanish. The simplified network is shown in Fig. 5, which is similar to that obtained when single-post obstacle equivalent circuits for the individual posts are used and are coupled by a length L of the waveguide.

The Coplanar Case: The procedure follows the general case up to the derivation of the network of Fig. 2. But for $L = 0$ the T network $Z(abc)$ of Fig. 2 cannot be transformed to a π network since the determinant of the Z matrix is zero. However, the (1,0) waveguide port can be isolated by using a transformer equivalent network [3]. When all the higher order modes and gap terminations are taken into account, the obstacle network of Fig. 6 is obtained. Delta-star transformation of the admittance elements $Y_A + Y_{G1}$, Y_B, $Y_C + Y_{G2}$ and further simplification

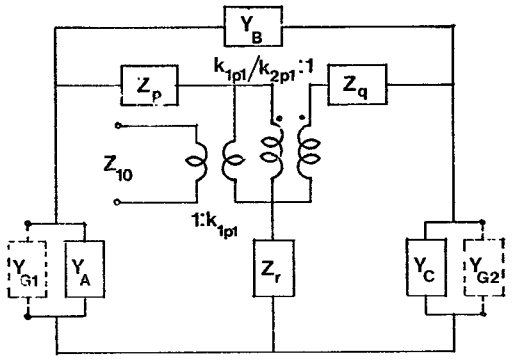

Fig. 6. Coupling network between the two-gap ports for the two-post coplanar configuration ($L = 0$). The (1,0) mode pair impedance port has been isolated.

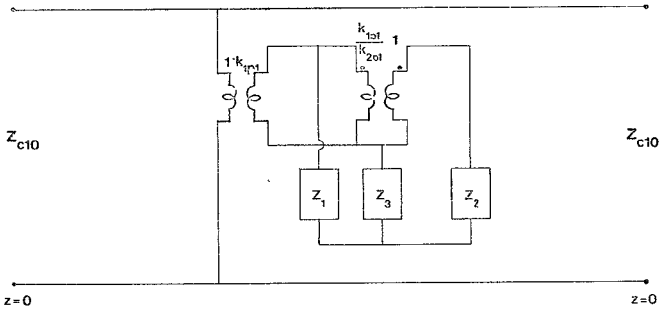

Fig. 7. Obstacle network representation of the coplanar configuration ($L = 0$) to the incident H_{10} mode in the waveguide.

leads to the obstacle representation of Fig. 7. The shunt obstacle admittance is given by

$$Y_{obs} = \frac{1}{Z_{obs}} = \frac{Z_1 k_{2p1}^2 + Z_2 k_{1p1}^2 + Z_3(k_{1p1} - k_{2p1})^2}{Z_1 Z_2 + Z_2 Z_3 + Z_3 Z_1} \quad (3)$$

where

$$Z_1 = Z_p + \frac{Y_C + Y_{G2}}{\Delta}$$

$$Z_2 = Z_q + \frac{Y_A + Y_{G1}}{\Delta}$$

$$Z_3 = Z_r + \frac{Y_B}{\Delta}$$

and

$$\Delta = (Y_A + Y_{G1})Y_B + (Y_C + Y_{G2})Y_B + (Y_C + Y_{G2})(Y_A + Y_{G1}).$$

The Single-Post Dual-Gap Structure

The admittance matrix elements given by (2) can be used to construct the coupling network between the gap ports for the nth spatial harmonic mode. Since admittance elements are involved, then π coupling networks are more suitable. The elements of such a π network represent coupling to all the waveguide mode pair impedance ports from $m = 1$ to ∞ for a fixed value of n. The coupling is dependent on the post coupling factor k_{pm} and the gap coupling factors k_{1gn} and k_{2gn}. For a general location of the two gaps, all the various (m,n) mode pair impedances for a fixed n value will be coupled to the three admittance elements. However, by symmetrically positioning the gaps it is possible to decouple a whole set of n modes (composed of all m values) [4]. This can be compared with the two-post symmetrical coplanar case.

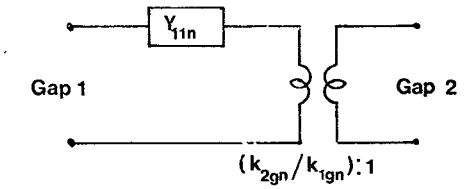

Fig. 8. Gap coupling network representation of Fig. 1(b) for an nth spatial harmonic.

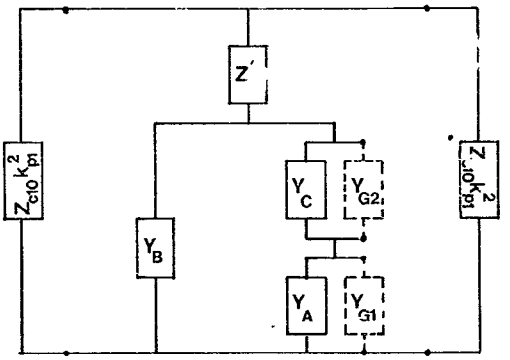

Fig. 9. Obstacle network representation of the post configuration of Fig. 1(b) to the incident H_{10} mode in the waveguide.

The physical fact that the two gaps are connected in series can be established from an alternative network representation. The determinant of the admittance matrix for each n is always zero, thus the network can be represented by the transformer coupled system shown in Fig. 8, which shows that the two-gap ports are connected in series through the admittance Y_{11n} and a transformer of ratio $(k_{2gn}/k_{1gn}) : 1$.

Post Structure Obstacle Representation

The complete network between the gap ports is composed of all the π networks for $n = 0$–∞ connected in parallel, and the post structure obstacle impedance to the H_{10} mode in infinite guide can be obtained along similar lines to that used for the general two-post case. The obstacle representation is shown in Fig. 9 with the following parameters:

$$Z_p' = \sum_{m=2}^{\infty} Z_{m0} k_{pm}^2$$

$$Y_A = \sum_{n=1}^{\infty} \left[\left\{ \sum_{m=1}^{\infty} Z_{mn} \left(\frac{k_{pm}}{k_{1gn}} \right)^2 \right\}^{-1} - \left\{ \sum_{m=1}^{\infty} Z_{mn} \left(\frac{k_{pm}^2}{k_{1gn} k_{2gn}} \right) \right\}^{-1} \right]$$

$$Y_B = \sum_{n=1}^{\infty} \left[\sum_{m=1}^{\infty} Z_{mn} \left(\frac{k_{pm}^2}{k_{1gn} k_{2gn}} \right) \right]^{-1}$$

$$Y_C = \sum_{n=1}^{\infty} \left[\left\{ \sum_{m=1}^{\infty} Z_{mn} \left(\frac{k_{pm}}{k_{2gn}} \right)^2 \right\}^{-1} - \left\{ \sum_{m=1}^{\infty} Z_{mn} \left(\frac{k_{pm}^2}{k_{1gn} k_{2gn}} \right) \right\}^{-1} \right].$$

$Y(ABC)$ represents the parallel addition of all the networks for $n > 0$ while Z_p' represents the remainder of the $(m,0)$ terms for $m \geq 2$. Y_{G1} and Y_{G2} are gap terminating admittances. The shunt obstacle is given by

$$Z_{obs} = \frac{1}{Y_{obs}} = \frac{1}{k_{p1}^2}\left\{Z_p' + \frac{1}{Y_B + \dfrac{(Y_A + Y_{G1})(Y_C + Y_{G2})}{Y_A + Y_{G1} + Y_C + Y_{G2}}}\right\}.$$

Experimental Measurements

The two-port coupling network representations of the general two-post two-gap and the single-post two-gap mounting configuration presented earlier represent coupling between the two-gap ports and the various mode pair impedance ports associated with the waveguide. These networks can be defined in the form of a T or a π network and are, in general, composed of three independent immittance elements. The convergence properties of the immittance elements are similar to those discussed in [5].

A direct verification of such a network model is possible along the lines adopted by Eisenhart and Khan [5]. However, in this case the network is characterized by three immittance elements rather than the one element required for the single-post single-gap case. Thus for a given post structure considered here it would be necessary to conduct a minimum of three measurements at one frequency at a gap port with the other gap port terminated in precisely known impedances. The impedance or admittance matrix elements will then have to be calculated from these measured results. Quite elaborate mechanical arrangements would be necessary for the implementation of this technique.

The alternative technique of measuring the impedance of the post structure as an obstacle to the incident H_{10} mode has been used here for the experimental verification of the theoretical model. The impedance at one waveguide port is measured with the second waveguide port and the two-gap ports appropriately terminated. Standard waveguide slotted-line impedance measuring techniques have been used. This simple and convenient means for the verification of the theoretical model has previously been used [2], [4], [5]. The post diameters and gap sizes selected in the experimental work were such that the limitations on w/a, g/b were not violated.

Two-Post Structure

The post structure obstacle representation for the dominant H_{10} mode for the general two-post two-gap configuration is composed of impedance and admittance elements representing summation over m and n values. For computational purposes the summation for m values is up to $M_1 = a/w_i$ where $w_i = 1.8d_i$ is the smaller of the two strip widths. The summation for n values is up to $N_1 = b/g_i$ where g_i is the smaller of the two gap dimensions. In order to avoid any error due to premature truncation of the series [5] for the $n = 0$ impedance element values, the summation for m values is up to $2M_1$.

Also, in order to account for the deviations from the assumed uniform current density distributions across the

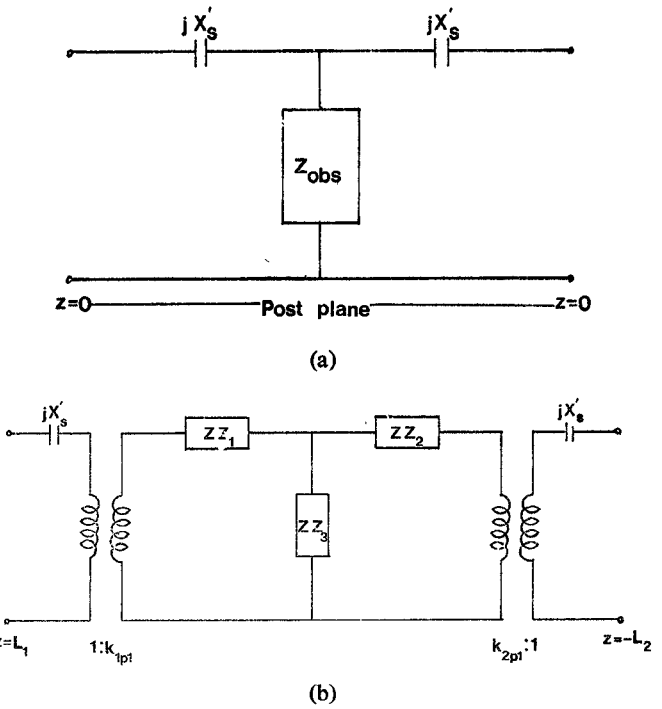

Fig. 10. Obstacle networks for the two-post configuration which take into account the effect of phase shifts introduced by the finite post diameters for (a) the coplanar case ($L = 0$) and (b) the staggered post case ($L \neq 0$).

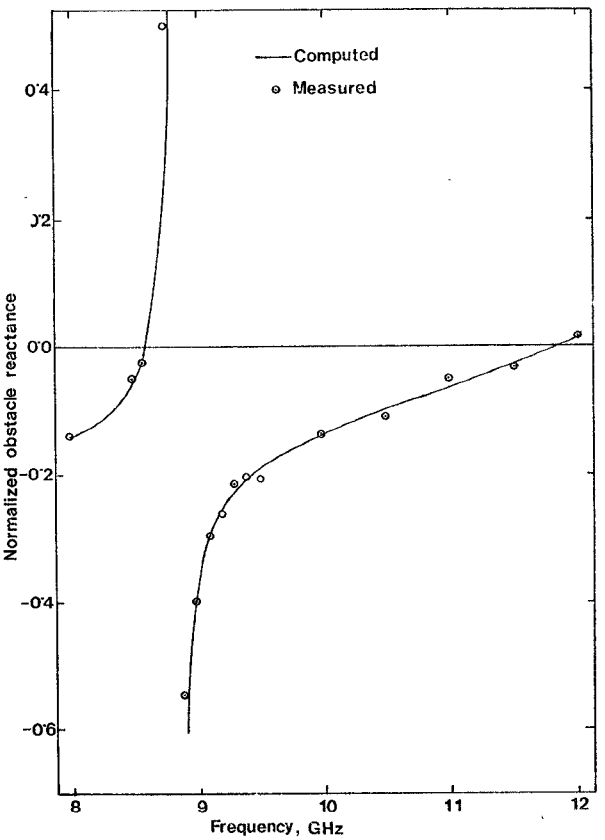

Fig. 11. Measured and computed values of the normalized shunt obstacle reactance for the two-post coplanar configuration. The parameters are as follows (all dimensions are in millimeters): waveguide: $a = 22.86$, $b = 10.16$. Post 1: $s_1 = 5.15$, $d_1 = 2.5$, $h_1 = 4.535$, $g_1 = 1.57$. Post 2: $s_2 = 12.21$, $d_2 = 1.5$, $h_2 = 8.535$, $g_2 = 1.03$. Post separation $L = 0.0$. The two gaps are air gaps.

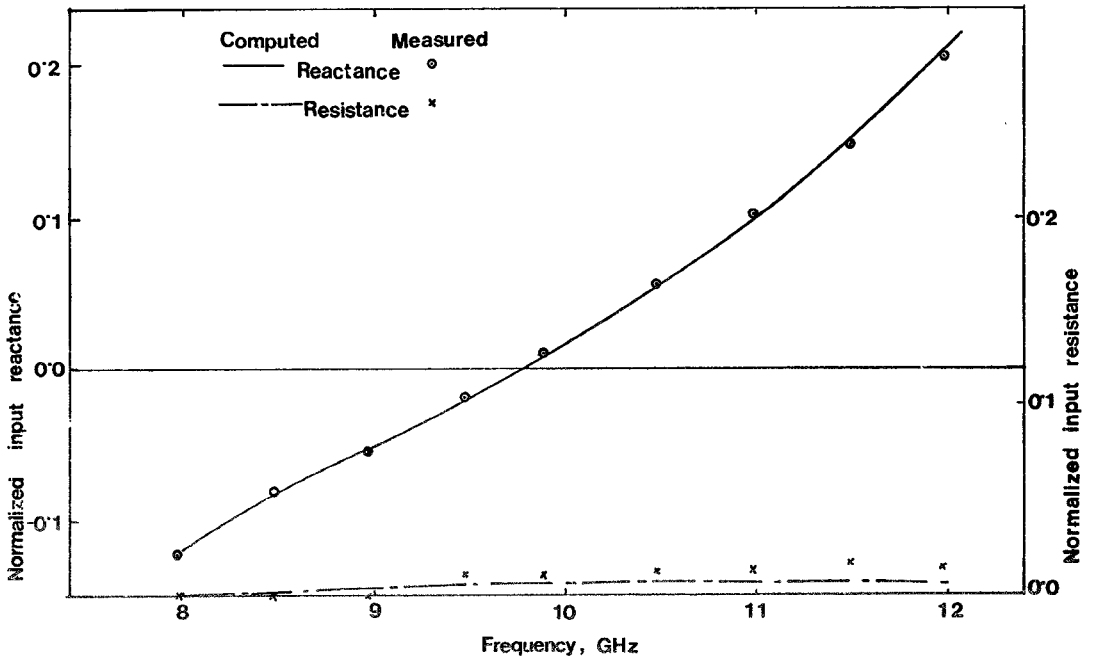

Fig. 12. Measured and computed values of the normalized input resistance and reactance for the staggered two-post configuration. The parameters are as follows (all dimensions are in millimeters): waveguide: $a = 22.86$, $b = 10.16$, Post 1: $s_1 = 7.125$, $d_1 = 2.95$, $h_1 = 9.125$, $g_1 = 1.71$. Post 2: $s_2 = 13.085$, $d_2 = 1.95$, $h_2 = 3.57$, $g_2 = 1.0$. Post separation: $L = 4.55$. The two gaps are air gaps. Measured and computed values refer to the post 1 plane.

two strips, correction factors $(1 - w_i/a)$ are used for the impedance elements Z_{ii0} for $i = 1,2$. The correction factor for the mutual impedance term is taken as

$$\left\{1 - \frac{(w_1 + w_2)}{4a}\right\}.$$

As will be seen later, these correction factors provide excellent agreement between the theory and experimental results. The correction factors used are not the same as those used in [2], and a comparison of the two factors when used to obtain the computed values is discussed in [6].

Coplanar Configuration: The obstacle representation for the coplanar post configuration is in the form of a shunt impedance element located at the $z = 0$ plane. The total obstacle network is shown in Fig. 10(a) in which the reactance jX_s' accounts for the phase shift introduced by the finite post diameters. The reactance jX_s' is the sum of the reactances due to each post, that is,

$$jX_s' = jX_{s1} + jX_{s2} \tag{4}$$

where [3]

$$jX_{si} = -jZ_{c10}\left(\frac{a}{\lambda_g}\right)\left(\frac{\pi d_i}{a}\right)^2 \sin^2\left(\frac{\pi s_i}{a}\right), \qquad i = 1,2 \tag{5}$$

for posts 1 and 2, respectively.

For the experimental work on the coplanar post configuration, one waveguide port was terminated in a matched load and impedance measured at the other port. The obstacle shunt reactance was then calculated from the measured impedance at the post plane and the computed value of the series reactance jX_s'.

Staggered Post Configuration: The staggered post arrangement is represented by a general two-port network, the two waveguide ports being coincident with the post axes location (Fig. 3). Because the length L of the waveguide and the two posts are replaced by an equivalent two-port network, the effect of finite phase shift is accounted for in an analogous manner. The total obstacle network is shown in Fig. 10(b), in which the network of Fig. 3 less the two transformers has been replaced by an equivalent T network. The phase shift reactance jX_s' is again given by (4).

For the experimental work on the staggered post configuration, the input impedance at one waveguide port was measured with the other port terminated in a matched load. This measured value was compared with the theoretical value given by the obstacle representation. This procedure was preferred to the alternative of having to determine the three elements of the network of Fig. 10(b).

Experimental Results: The results on the two-post configurations are indicated in Figs. 11–13. In all these post structures no external material was used to fill the two gaps. Thus the gap terminating impedance was that corresponding to the parallel-plate capacitance with air as the dielectric material. Fringing effects were not included. It can be seen that excellent agreement between the computed and measured values of the obstacle shunt reactance has been obtained for the coplanar configuration (Fig. 11). For staggered post arrangements (Figs. 12 and 13) very good agreement between the measured and computed input impedance values has been obtained in all cases. It is worth pointing out that Fig. 13(a) and (b) refers to the same staggered post configuration but measured at the two different waveguide

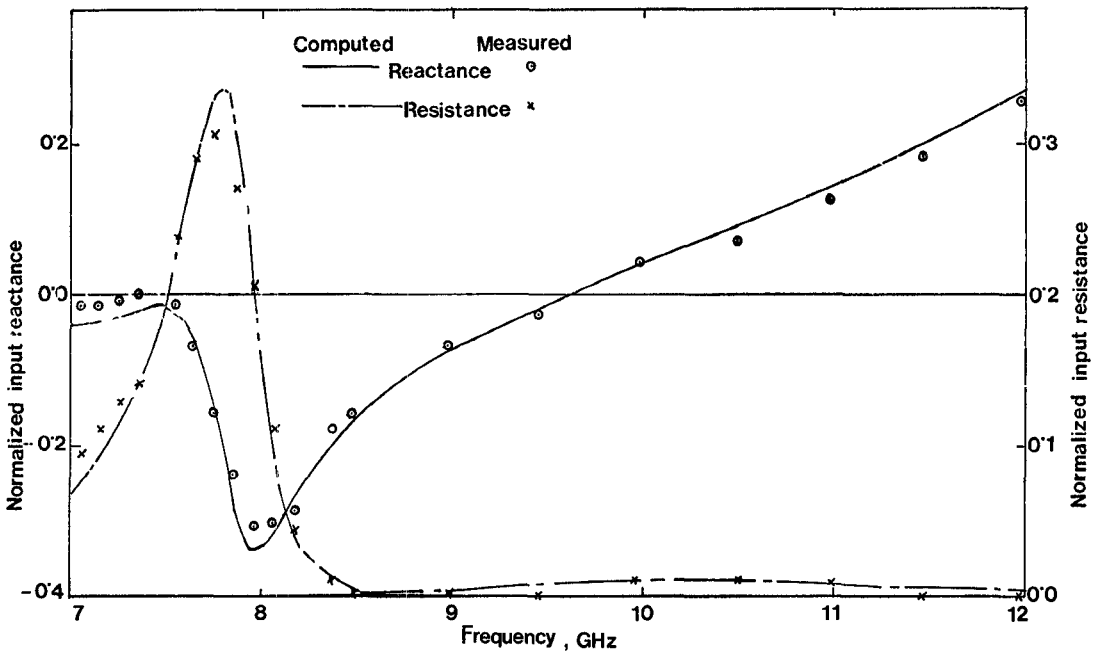

(a)

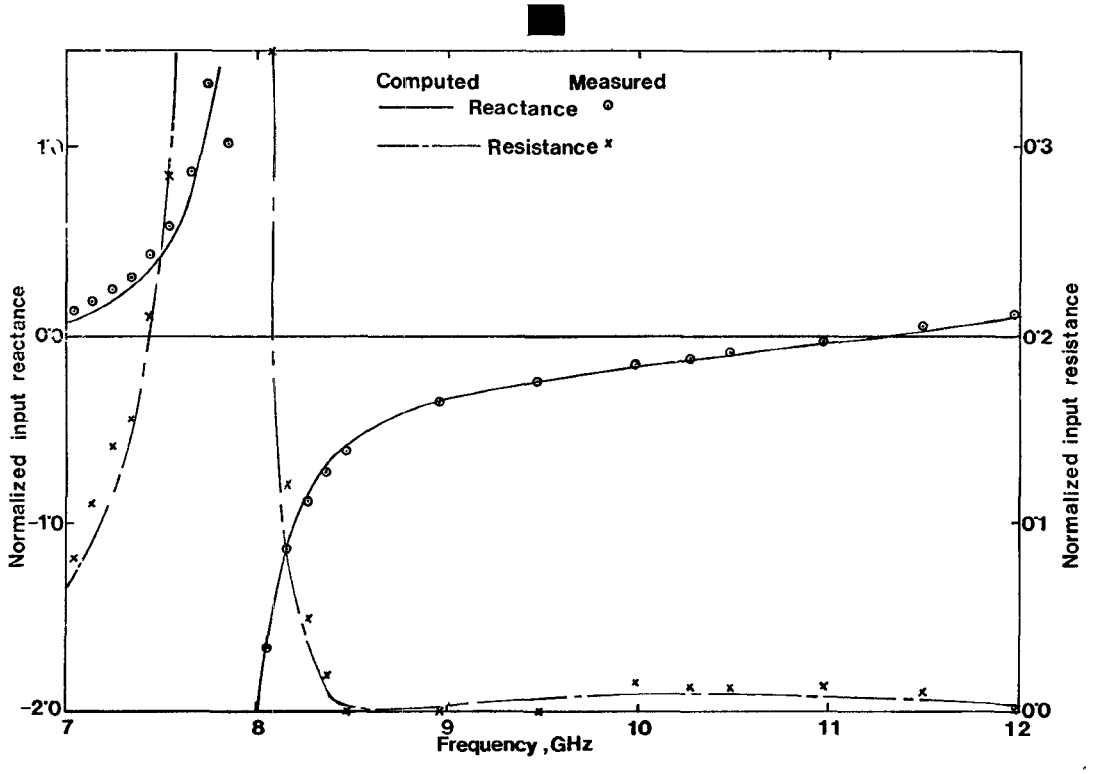

(b)

Fig. 13. Measured and computed values of the normalized input resistance and reactance for the staggered two-post configuration. The parameters are as follows (all dimensions are in millimeters): waveguide: $a = 22.86$, $b = 10.16$. Post 1: $s_1 = 9.27$, $d_1 = 1.0$, $h_1 = 2.0$, $g_1 = 0.8$. Post 2: $s_2 = 14.075$, $d_2 = 1.6$, $h_2 = 4.585$, $g_2 = 0.87$. Post separation: $L = 4.70$. The two gaps are air gaps. Measured and computed values refer to (a) the post plane 1 and (b) the post plane 2.

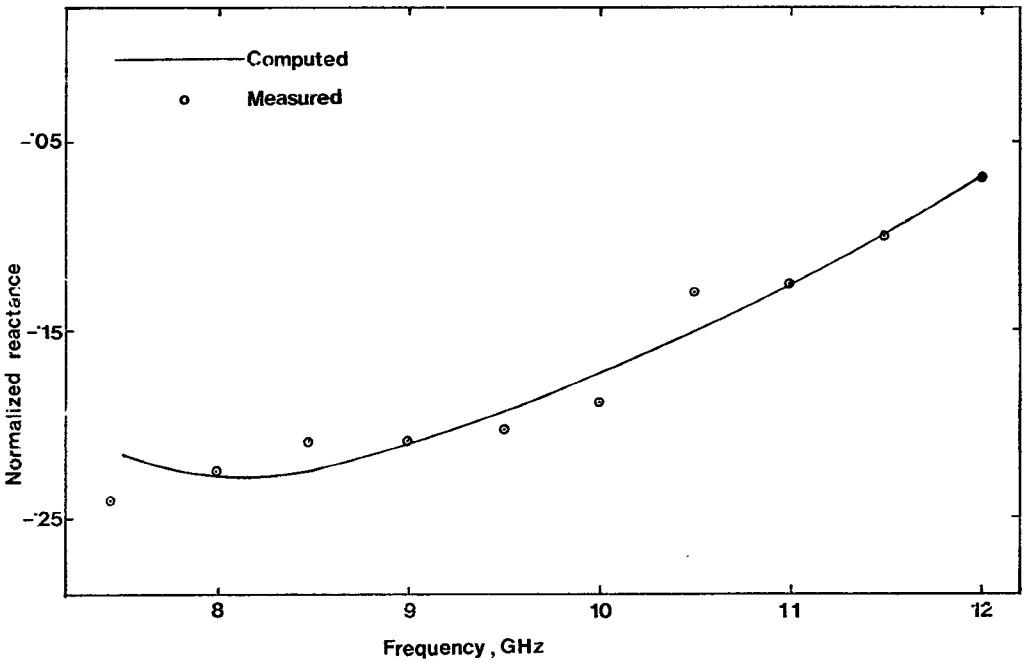

Fig. 14. Measured and computed values of the normalized shunt obstacle reactance for the single-post two-gap configuration. The parameters are as follows (all dimensions are in millimeters): waveguide: $a = 22.86$, $b = 10.16$. Post: $s = 10.8$, $d = 2.76$. Gap 1: $h_1 = 2.485$, $g_1 = 0.63$. Gap 2: $h_2 = 6.05$, $g_2 = 0.9$. Gap 1 contains a 2.3-mm diam circular alumina disk (dielectric constant = 10) while gap 2 is an air gap.

ports. The resonance seen in Fig. 11 occurs when in (3)

$$Z_1 k_{2p1}^2 + Z_2 k_{1p1}^2 + Z_3 (k_{1p1} - k_{2p1})^2 = 0.$$

The series element ZZ_2 of Fig. 7 tends to ∞ near 7.8 GHz. This decouples waveguide port 2 resulting in a finite reactance measured at port 1 [Fig. 13(a)]. When measured at port 2 the reactance goes to ∞ as shown in Fig. 13(b).

Single-Post Two-Gap Configuration

The post structure obstacle representation for the dominant H_{10} mode for the single-post two-gap configuration is composed of immittance elements representing summation over m and n values. For computational purposes, the summation over m values is up to $M_1 = a/w$ where $w = 1.8d$. The summation over n values is up to $N_1 = b/g_i$ where g_i ($i = 1,2$) is the smaller of the two gap dimensions. Similar to [4], [5] for the impedance element Z_p', corresponding to $n = 0$, the summation for m values is up to $2M_1$ with a correction factor $(1 - w/a)$.

The total obstacle representation of the post configuration at the $z = 0$ plane for the incident H_{10} mode is the same as that in Fig. 10(a), except that in this case the effect of phase shift introduced by the finite post diameter is accounted for by the phase shift reactance jX_s given by (5) with appropriate parameters for the single post. The experimental procedure for this structure was the same as that for the two-post coplanar arrangement.

The theoretical and experimental results on such a configuration are indicated in Fig. 14. In this configuration one gap was partially filled with a 0.025-in-thick circular alumina piece while the other was an air gap. Again the gap terminating impedances were those corresponding to the appropriate parallel plate capacitances. It can be seen that good agreement between measured and computed values is obtained.

The theoretical model, however, does not take losses associated with the system into account. The use of air gaps in the two-post structures has, however, kept these losses to a minimum, resulting in an excellent agreement between the measured and computed results. The addition of an alumina disk, which is necessary for the single-post two-gap configuration, has, however, introduced extra losses in the system and would probably account for the slight discrepancy observed in this case.

Conclusion

A unified network representation for the dual-gap waveguide post configurations which are of practical importance has been presented and discussed. The agreement between values computed from the results of the analysis and the measurements on the double-gap structures should give confidence in the subsequent use of the method for evaluating microwave systems using these structures. Of particular interest are those arrangements where semiconductor devices are mounted in the gaps, for example, a double-gap system covering the case of a varactor-tuned Gunn or IMPATT device.

References

[1] J. S. Joshi and J. A. F. Cornick, "Analysis of waveguide post configurations: Part I—Gap Immittance Matrices," this issue, pp. 169–173.

[2] O. L. El-Sayed, "Impedance characterization of a two-post mounting structure for varactor tuned Gunn-oscillators," *IEEE Trans. Microwave Theory Tech.*, vol. MTT-22, pp. 769–776, Aug. 1974.

[3] N. Marcuvitz, *Waveguide Handbook* (MIT Rad. Lab. Ser., vol. 10). New York: McGraw-Hill, 1951.
[4] J. S. Joshi and J. A. F. Cornick, "Analysis of a waveguide mounting configuration for electronically tuned transferred-electron-device oscillators and its circuit application," *IEEE Trans. Microwave Theory Tech.*, vol. MTT-24, pp. 573–584, Sept. 1976.
[5] R. L. Eisenhart and P. J. Khan, "Theoretical and experimental analysis of a waveguide mounting structure," *IEEE Trans. Microwave Theory Tech.*, vol. MTT-19, pp. 706–719, Aug. 1971.
[6] J. S. Joshi, "Analysis of general waveguide post configurations," Ph.D. dissertation, Council for National Academic Awards, London, May 1976.

Double Circulation Frequency Operation of Stripline *Y*-Junction Circulators

TSUKASA NAGAO, MEMBER, IEEE

Abstract—**The double circulation frequency operation (DCFO) of stripline *Y*-junction circulators loaded with dielectric–ferrite composites is presented. The dielectric–ferrite composite is made by combining a dielectric puck with a ferrite ring. The DCFO is identified in the mode chart, and it is found that mode 1 and mode 1A, according to Davies and Cohen, play their respective roles in the circulation. Theoretical results of perfect circulation are derived, applying Bosma's Green's function to the junction mode impedances, and then, design and operation of the DCFO are studied. Finally, experimental examples are presented.**

I. Introduction

THE stripline *Y*-junction circulator has long been widely used as one of the versatile microwave devices. It can be used as an isolator or as a switch, as well as a circulator. There are really many varieties of the circulator utilized: stripline and microstrip versions, *Y* and *X* junctions, wide-band and narrow-band uses, and so on. These varieties of the circulator are evidence that it has served various needs arising in microwave circuit design. Needless to say, it is practically important that these circulators are dealt with theoretically. As is known generally, some consistent theories are available about the elementary circulator. The design and the operating procedure of the circulator were developed by Bosma [1], [2], Davies and Cohen [3], and Fay and Comstock [4]. Many researchers have since demonstrated that they are conspicuously useful in making circulators, usually for narrow bandwidth use. If broad-banding circuits are utilized, then wide-band circulators are actually realized. Recently, Wu and Rosenbaum [5] have demonstrated that they are also effective in achieving an octave bandwidth operation of the circulator, without any broad-banding circuits.

However, it is worthwhile to note that all of these circulators are designed to operate at a single circulation frequency regardless of wide-band use or narrow-band use. Therefore, in the *Y*-junction circulators the dominant normal mode, especially mode 1 among the modes of perfect circulation, plays an essential role. As already noted by many people, a higher order mode operation is also available in a *Y* circulator or in an *X* circulator if it is adequately adjusted to its circulator conditions [3], [4], [6].

Some further efforts to enhance the versatility of the circulator have been made, which are related to the simultaneous operation of both the dominant mode and any other modes. It has not received much attention, though it is conceivably possible. There are a few examples, [7] and [8], referred to as simultaneous operation, in which one circulation takes place below the ferromagnetic resonance, and the other circulation takes place above the resonance in the sense opposite to that below the resonance. The operation of this type, however, is hard to deal with from the consistent theory of the elementary circulator because it does not hold beyond ferromagnetic resonance.

In this paper, apart from the simultaneous operation of both below-resonance and above-resonance circulations, the double circulation frequency operation (DCFO) is treated. DCFO is obviously another simultaneous operation which takes place exclusively above or below resonance, and which consists of both the dominant mode circulation and the other mode circulation. Only the DCFO above resonance is discussed.

The stripline *Y*-junction circulator used, as is shown in Fig. 1, is a stripline *Y* junction loaded with ring ferrites (dielectric–ferrite composites) in place of disk ferrites, and it is detached from any external tuning elements for the purpose of broad banding the circulator. The external magnetic field is applied parallel to the axis of the ring ferrites and the ferrite is biased beyond saturation.

To identify the DCFO, points of maximum isolation (isolation peak) are plotted superposed in the mode chart,

Manuscript received April 22, 1976; revised August 2, 1976.
The author is with the Department of Electrical Engineering, National Defense Academy, Yokosuka, Kanagawa 239, Japan.